Published in final edited form as:
J Am Chem Soc. 2008 April 2; 130(13): 4352–4363.

Iron Complexes of Dendrimer-Appended Carboxylates for Activating Dioxygen and Oxidizing Hydrocarbons

Min Zhao[†], **Brett Helms**[‡], **Elena Slonkina**[§], **Simone Friedle**[†], **Dongwhan Lee**[†], **Jennifer DuBois**[§], **Britt Hedman**[§], **Keith O. Hodgson**[§], **Jean M. J. Fréchet**[‡], and **Stephen J. Lippard**[†]
Department of Chemistry, Massachusetts Institute of Technology, 77 Massachusetts Avenue, Cambridge, Massachusetts 02139, Department of Chemistry, University of California, Berkeley, and Division of Materials Sciences, Lawrence Berkeley National Laboratory, Berkeley, California 94720 −1460, and Department of Chemistry and Stanford Synchrotron Radiation Laboratory, Stanford University, Stanford, California 94305

Abstract

The active sites of metalloenzymes are often deeply buried inside a hydrophobic protein sheath, which protects them from undesirable hydrolysis and polymerization reactions, allowing them to achieve their normal functions. In order to mimic the hydrophobic environment of the active sites in bacterial monooxygenases, diiron(II) compounds of the general formula $[Fe_2([G\text{-}3]COO)_4(4\text{-}RPy)_2]$ were prepared, where $[G\text{-}3]COO^-$ is a third-generation dendrimer-appended terphenyl carboxylate ligand and 4-RPy is a pyridine derivative. The dendrimer environment provides excellent protection for the diiron center, reducing its reactivity toward dioxygen by about 300-fold compared with analogous complexes of terphenyl carboxylate ($[G\text{-}1]COO^-$) ligands. An $Fe^{II}Fe^{III}$ intermediate was characterized by electronic, electron paramagnetic resonance, Mössbauer, and X-ray absorption spectroscopic analyses following the oxygenation of $[Fe_{2-}([G\text{-}3]COO)_4(4\text{-}PPy)_2]$, where 4-PPy is 4-pyrrolidinopyridine. The results are consistent with the formation of a superoxo species. This diiron compound, in the presence of dioxygen, can oxidize external substrates.

Introduction

The active sites of metalloenzymes are often surrounded by a hydrophobic sheath of amino acids that shields them from undesirable hydrolysis and polymerization reactions and facilitates their normal functions. Dendrimers are highly branched molecules with well-defined 3-D structures. As in metalloenzymes, a site-isolated environment can be provided by dendrons arranged to protect a core moiety from unwanted side reactions.[1] This distinctive property of dendrimers makes them excellent candidates to mimic a hydrophobic metalloprotein core framework. Dendritically functionalized iron(II) porphyrins are able to bind O_2 reversibly and model the chemistry of heme proteins.[2] In addition, a porphyrin compound with a dendrimer at its periphery exhibited size and shape selectivity due to cavities formed within the dendrons.[3] A dendrimer-derived mimic of a non-heme diiron protein was achieved when modified triazacyclononanes were used as ligands to prepare diiron(III) complexes, which could be reduced to their diiron(II) forms upon irradiation.[4] The fourth-generation dendrimer diiron(III) compound used in this work was highly robust against alkaline hydrolysis, demonstrating that the dendrons stabilize the active site just as do hydrophobic protein frames.

E-mail: frechet@berkeley.edu; lippard@mit.edu.
[†]Massachusetts Institute of Technology.
[‡]University of California, Berkeley.
[§]Stanford University.

Terphenyl carboxylate ligands recently developed in our laboratory[5,6] and elsewhere[7] form diiron(II) complexes that closely resemble the active site of the hydroxylase of soluble methane monooxygenase (MMOH) in its reduced state. In the presence of dioxygen, several of these complexes convert to di(μ-hydroxo)diiron(III) species that mimic the oxidized state of MMOH.[6,8–12] In some of this chemistry, the formation of peroxodiiron(III) and/or di(μ-oxo)diiron (IV) intermediates was suggested, although no direct evidence for such species was obtained.[6]

In the present study we have modified the terphenyl carboxylate ligand framework to incorporate a dendrimer sheath by utilizing, in particular, a poly(benzylether) carboxylic acid [G-3]-COOH (**7**). Because of the dendritic polybenzylether units and terminal long-chain alkyl groups of **7**, we anticipated that its diiron complexes would be highly soluble in a variety of organic solvents and that the dimetallic center would be well protected. Our previous research on diiron model compounds revealed that oxygenated intermediates could often be observed at low temperatures, $T < -78$ °C. With the dendritic shield, we envisaged increased thermal stability, since solvent and substrate access is more restricted, and that we would more readily be able to investigate the structure and reactivity of these intermediates.

Experimental Section

General Considerations

All reagents were purchased from commercial sources and used as received except for Fe(OTf)$_2$·2MeCN,[13] 2,6-dibromo-3,5-dihydroxybenzoic acid,[14] [Fe$^{II}_2$(μ-O$_2$CAr^{Tol})$_2$(O$_2$CAr^{Tol})$_{2-}$(Py)$_2$] (**A**),[5] [Fe$^{II}_2$(μ-O$_2$CAr^{Tol})$_4$(*t*-Bu-Py)$_2$] (**B**),[8] and [Fe$^{III}_2$(μ-OH)$_2$(μ-O$_2$CAr^{Tol})$_2$(O$_2$CAr^{Tol})$_2$(*t*-Bu-Py)$_2$](**C**),[8] which were prepared according to literature procedures. All solvents were saturated with nitrogen and purified by passage through activated Al_2O_3 columns under nitrogen. Air-sensitive manipulations were performed under nitrogen in an MBraun glovebox.

Physical Measurements

^{1}H NMR spectra were recorded on Inova 300 MHz and Bruker 500 MHz DRX spectrometers. Chemical shifts were referenced to residual deuterated solvent peaks. FT-IR spectra were recorded on an Avatar 360 FT-IR instrument, and samples were prepared as KBr pellets. UV–vis spectra were recorded on a Hewlett-Packard 8453 diode array spectrophotometer. ESI-MS spectrometry was performed with an Agilent 1100 Series LC/MSD system. MALDI-TOF mass spectrometry was performed on a Voyager-DE instrument from PerSeptive Biosystems using α-cyanohydroxycinnamic acid as a matrix. FAB and EI mass spectrometry was performed by the UC Berkeley mass spectrometry facility.

tert-Butyl 2,6-Dibromo-3,5-dihydroxybenzoate (1)

A solution containing 2,6-dibromo-3,5-dihydroxybenzoic acid (3.12 g, 10 mmol), di-*tert*-butyl dicarbonate (8.72 g, 40 mmol), and magnesium perchlorate (22 mg, 0.1 mmol) in 50 mL of nitromethane and 50 mL of acetone was heated at 40 °C for 16 h. The reaction mixture was then diluted with 200 mL of ethyl acetate and washed successively with saturated NH_4Cl, saturated $NaHCO_3$, water, and brine. The organic layer was dried over $MgSO_4$ and concentrated. The residue was purified by column chromatography using an ethyl acetate/hexanes gradient of 1:2 to 2:1 (v/v). The product was obtained as a colorless solid (1.84 g, 50%). ^{1}H NMR (acetone-d_6) δ (ppm): 9.2 (br, 2H), 6.75 (s, 1H), 1.60 (s, 9H). ^{13}C NMR (acetone-d_6) δ (ppm): 164.4, 154.2, 139.8, 103.5, 96.7, 82.9, 27.3. FT-IR (cm^{-1}): 3469, 3158, 2980, 2930, 2810, 2666, 2579, 2493, 1690, 1576, 1476, 1453, 1424, 1385, 1368, 1337, 1294, 1248, 1157, 1065, 1045, 971, 834, 807, 739, 690. LR-MS (FAB), Calcd for $C_{11}H_{12}Br_2O_4$: *m*/*z* 366. Found: *m*/*z* 367 ([M + H]$^+$, 30), 312(30), 295(15), 154(100), 136(75). HR-MS (FAB),

Calcd for $C_{11}H_{12}Br_2O_4$: *m*/*z* 365.9102. Found: *m*/*z* 365.9110. Anal. Calcd for $C_{11}H_{12}Br_2O_4$: C, 35.90; H, 3.29. Found: C, 36.20; H, 3.36.

tert-Butyl 2,6-Dibromo-3,5-di(benzyloxy)benzoate (2)

A portion of benzyl bromide (2.08 g, 12.2 mmol), **1** (2.00 g, 5.42 mmol), and 18-crown-6 (284 mg, 1.08 mmol) were dissolved in 40 mL of acetone. To this solution was added finely pulverized anhydrous K_2CO_3 (4.50 g, 32.6 mmol). After 16 h at gentle reflux, the reaction mixture was cooled to room temperature and diluted with ethyl acetate, filtered, and concentrated. The product was obtained as colorless needles (2.85 g, 96%) after recrystallization from a mixture of hexane and ethyl acetate (15:1, v/v). ^{1}H NMR ($CDCl_3$) δ (ppm): 7.38–7.32 (m, 10H), 6.50 (s, 1H), 5.06 (s, 4H), 1.64 (s, 9H). ^{13}C NMR ($CDCl_3$) δ (ppm): 164.7, 155.1, 140.0, 135.8, 128.8, 128.3, 127.0, 101.2, 101.1, 84.1, 71.5, 28.1. FT-IR (cm^{-1}): 3087, 3065, 3032, 2978, 2932, 2875, 1730, 1572, 1497, 1454, 1437, 1392, 1369, 1337, 1246, 1226, 1198, 1157, 1089, 1047, 1027, 908, 843, 810, 791, 735, 697. LR-MS (EI), Calcd for $C_{25}H_{24}Br_2O_4$: *m*/*z* 546. Found: *m*/*z* 546 ($[M]^+$, 20), 494(30), 492(15), 475(80), 473(40), 458 (20), 456(10), 402(60), 400(30), 385(40), 383(20), 91(100). HR-MS (EI), Calcd. for $C_{25}H_{24}Br_2O_4$: *m*/*z* 546.0041. Found: *m*/*z* 546.0046. Anal. Calcd for $C_{25}H_{24}Br_2O_4$: C, 54.77; H, 4.41. Found: C, 54.40; H, 4.65.

tert-Butyl 3,5-Di(benzyloxy)-2,6-diphenylbenzoate (3)

A reaction mixture containing **2** (3.87 g, 7.05 mmol), phenylboronic acid (12.9 g, 106 mmol), $Pd(PPh_3)_4$ (2.03 g, 1.76 mmol), and K_3PO_4 (30.0 g, 141 mmol) in 150 mL of dry 1,2-dimethoxyethane was subjected to three freeze–pump–thaw cycles before heating at 95 °C for 72 h under an argon atmosphere. The crude mixture was diluted with diethyl ether and then extracted successively with saturated NH_4Cl, saturated $NaHCO_3$, water, and then brine. The organic layer was dried over $MgSO_4$ and concentrated. The product was obtained as a colorless solid (2.75 g, 72%) after column chromatography using a gradient of 4:1 (v/v) chloroform/hexanes to chloroform. Recrystallization from hexanes yielded colorless needles. ^{1}H NMR ($CDCl_3$) δ (ppm): 7.40–7.25 (m, 16H), 7.16 (d, 2H, *J* 6.8 Hz), 6.66 (s, 1H), 4.96 (s, 4H), 0.95 (s, 9H). ^{13}C NMR ($CDCl_3$) δ (ppm): 166.8, 155.6, 138.1, 136.9, 135.9, 130.5, 128.4, 127.6, 127.6, 127.0, 126.7, 122.1, 101.0, 81.5, 70.8, 27.2. FT-IR (cm^{-1}): 3087, 3061, 3030, 2974, 2931, 2875, 1723, 1602, 1585, 1497, 1454, 1368, 1325, 1303, 1255, 1222, 1169, 1083, 1051, 1029, 910, 849, 830, 818, 790, 762, 736, 698. LR-MS (FAB), Calcd for $C_{37}H_{34}O_4$: *m*/*z* 542. Found: *m*/*z* 543 ($[M + H]^+$, 100), 487(40), 469(25). HR-MS (FAB), Calcd for $C_{37}H_{34}O_4$: *m*/*z* 542.2457. Found: *m*/*z* 542.2459. Anal. Calcd for $C_{37}H_{34}O_4$: C, 81.89; H, 6.32. Found: C, 81.81; H, 6.51.

tert-Butyl 3,5-Dihydroxy-2,6-Diphenylbenzoate (4)

Hydrogenolysis of **3** (1.93 g, 3.55 mmol) was accomplished using a suspension of 10% Pd/C (200 mg) in 50 mL of a 1:1 (v/v) mixture of methanol and dichloromethane. The reaction vessel was evacuated and back-filled with hydrogen gas three times before stirring at ambient temperature for 16 h. The Pd/C was filtered though Celite, which was then washed several times with the same solvent mixture used in the reaction. After removal of the volatiles in vacuo, the product was obtained as a colorless solid (1.25 g, 97%) that required no further purification. ^{1}H NMR ($CDCl_3$) δ (ppm): 7.48−7.39 (m, 10H), 6.68 (s, 1H), 5.11 (s, 2H), 0.95 (s, 9H). ^{13}C NMR ($CDCl_3$) δ (ppm): 166.6, 153.3, 136.5, 133.7, 130.6, 129.1, 128.4, 118.3, 102.7, 81.6, 27.2. FT-IR (cm^{-1}): 3505, 3485, 3058, 3023, 3004, 2977, 2931, 2249, 1721, 1696, 1608, 1593, 1496, 1472, 1460, 1392, 1368, 1320, 1253, 1153, 1073, 1040, 968, 910, 848, 790, 764, 733, 702. LR-MS (FAB), Calcd for $C_{23}H_{22}O_4$: *m*/*z* 362. Found: *m*/*z* 362 ($[M]^+$, 100), 307 (90), 289(50). HR-MS (FAB), Calcd for $C_{23}H_{22}O_4$: *m*/*z* 362.1518. Found: *m*/*z* 362.1521. Anal. Calcd for $C_{23}H_{22}O_4$: C, 76.22; H, 6.12. Found: C, 76.12; H, 5.94.

[G-3]-Ester (6)

The second-generation bromide dendron **5**[15] (1.62 g, 1.44 mmol) was dissolved in 10 mL of acetone along with **4** (250 mg, 0.691 mmol) and 18-crown-6 (18 mg, 0.068 mmol). To this solution was added finely pulverized anhydrous K_2CO_3 (571 mg, 4.14 mmol). After 16 h at gentle reflux, the reaction mixture was cooled and diluted with ethyl acetate, filtered, and concentrated. The product was obtained as a colorless glass (1.67 g, 99%) after column chromatography using a mixture of hexane and ethyl acetate (15:1, v/v) as eluent. ^{1}H NMR ($CDCl_3$) δ (ppm): 7.44 (d, 4H, *J* 7.2 Hz), 7.37 (t, 4H, *J* 7.3 Hz), 7.29 (t, 2H, *J* 7.2 Hz), 6.75 (s, 1H), 6.53 (s, 8H), 6.49 (s, 2H), 6.44 (s, 4H), 6.41 (s, 4H), 4.98 (s, 4H), 4.79 (s, 8H), 3.93 (t, 16H, *J* 6.6 Hz), 1.76 (m, 16H), 1.42 (m, 16H), 1.26 (m, 128H), 0.94 (s, 9H), 0.88 (t, 24H, *J* 6.8 Hz). ^{13}C NMR ($CDCl_3$) δ (ppm): 166.7, 160.5, 160.0, 155.8, 139.2, 138.9, 138.0, 136.0, 130.7, 127.6, 127.0, 122.0, 105.7, 104.9, 101.6, 100.7, 100.0, 81.5, 70.5, 70.0, 68.0, 31.9, 29.63, 29.60, 29.58, 29.56, 29.39, 29.31, 29.25, 26.0, 22.7, 14.1. FT-IR (cm^{-1}): 2923, 2853, 1725, 1597, 1450, 1377, 1331, 1289, 1258, 1160, 1057, 830, 720, 698, 673. LR-MS (MALDI-TOF): Calcd. for $C_{161}H_{250}O_{16}$: *m*/*z* 2439.9; Found: *m*/*z* 2462.4 ($[M + Na]^+$, 100). Anal. Calcd for $C_{161}H_{250}O_{16}$: C, 79.20; H, 10.32. Found: C, 79.53; H, 10.59.

[G-3]-COOH (7)

Thermolysis of **6** (1.50 g, 0.614 mmol) was performed in 10 mL of quinoline at 220 °C for 16 h. The reaction mixture was diluted with 50 mL of ethyl acetate, washed with 2.0 M HCl (5 × 25 mL), dried, and concentrated. The title compound was obtained as a pale brown glass (1.40 g, 96%) after column chromatography using a mixture of hexane and ethyl acetate (9:1, v/v). ^{1}H NMR ($CDCl_3$) δ (ppm): 7.44 (d, 4H, *J* 7.2 Hz), 7.37 (t, 4H, *J* 7.2 Hz), 7.32 (t, 2H, *J* 7.2 Hz), 6.76 (s, 1H), 6.53 (s, 8H), 6.49 (s, 2H), 6.44 (s, 4H), 6.41 (s, 4H), 4.98 (s, 4H), 4.79 (s, 8H), 3.92 (t, 16H, *J* 6.6 Hz), 1.76 (m, 16H), 1.42 (m, 16H), 1.26 (m, 128H), 0.88 (t, 24H, *J* 6.8 Hz). ^{13}C NMR ($CDCl_3$) δ (ppm): 168.9, 160.5, 160.0, 155.9, 139.1, 138.9, 135.7, 135.4, 130.4, 127.9, 127.4, 122.3, 105.8, 105.0, 101.7, 100.8, 70.6, 70.1, 68.1, 32.0, 29.71, 29.67, 29.66, 29.63, 29.46, 29.39, 29.32, 26.1, 22.7, 14.2. FT-IR (cm^{-1}): 2922, 2853, 1702, 1599, 1451, 1375, 1327, 1219, 1158, 1051, 920, 849, 830, 772, 704, 682. LR-MS (MALDI-TOF), Calcd for $C_{157}H_{242}O_{16}$: *m*/*z* 2383.8. Found: *m*/*z* 2410.7 ($[M + Na]^+$, 100), 2426.6 ($[M + K]^+$, 20). Anal. Calcd for $C_{157}H_{242}O_{16}$: C, 79.09; H, 10.22. Found: C, 79.21; H, 10.37.

[G-3]-COONa (8)

Compound **7** (130 mg, 54.5 μmol) was dissolved in 4 mL of THF, and to this solution was added 19 μL of 3 N aq NaOH, followed by 1 mL of MeOH to make the reaction mixture homogeneous. The solution was allowed to reflux for 5 h. The solvents were then removed under reduced pressure. The residue was dissolved in pentane and filtered through Celite. Pentane was evaporated to afford a light yellow solid, which was dried under vacuum at 80 °C overnight to yield 136 mg of product (100% yield). FT-IR (cm^{-1}): 2923 (s), 2853 (m), 1599 (s), 1574 (s), 1456 (m), 1375 (m), 1326 (w), 1169 (s), 1055 (m), 830 (m), 761 (w), 722 (w), 700 (w), 682 (w). ^{1}H NMR ($CDCl_3$) δ (ppm): 7.47 m, (4H), 7.28 (m, 6H), 6.71 (s, 1H), 6.60 (d, 8H), 6.55 (s, 2H), 6.47 (s, 8H), 4.98 (s, 4H), 4.83 (s, 8H), 3.97 (t, 16H), 1.83 (m, 16H), 1.51 (m, 16H), 1.36 (m, 128H), 0.98 (t, 24H). LR-MS (ESI), Calcd for $C_{157}H_{241}O_{16}Na$: *m*/*z* 2406. Found: *m*/*z* 2383 ($[M – Na]^-$, 100)

$[Fe_2([G\text{-}3]COO)_4(4\text{-}RPy)_2]$ (9-R)

Compound **8** (96.2 mg, 40.0 μmol) and $Fe(OTf)_2 \cdot 2MeCN$ (10.9 mg, 25.0 μmol) were mixed in THF and stirred at room temperature for 10 h. The volatile fraction was removed in vacuo, and the residue was dissolved in pentane. Insoluble materials were filtered off. Excess 4-R-pyridine (4-cyanopyridine, 4-CNPy; or 4-pyrrolidinopyridine, 4-PPy) was then added to the yellow filtrate, and the mixture was stirred vigorously for 2 h. Solvent was removed, pentane

(2 mL) was added to dissolve the dendrimer product, and the solution was filtered. These procedures were repeated three times to afford the diiron(II) products as a red (for 4-CNPy) or yellow (for 4-PPy) sticky solid. **9**-CN: Yield 95%. An ^{57}Fe-enriched sample of **9**-P was prepared from ^{57}Fe-enriched (40%) $Fe(OTf)_2{\cdot}2MeCN$, which was synthesized by reaction of triflic acid with a mixture of ^{57}Fe and natural Fe powder (2:3, w/w).[13] FT-IR (cm^{-1}): 2924 (s), 2853 (s), 2238 (w, $\nu_{C\equiv N}$), 1598 (s), 1454 (m), 1378 (m), 1323 (m), 1167 (s), 1054 (m), 830 (m) 765 (w), 721 (w), 703 (w), 682 (w). Anal. Calcd for $C_{640}H_{992}N_4O_{74}Fe_2$ (**9**-CN + $10H_2O$): C, 76.57; H, 9.96; N, 0.56. Found: C, 76.58; H, 9.86; N, 0.64. **9**-P: Yield 90%. FT-IR (cm^{-1}): 2923 (s), 2853 (s), 1599 (s), 1559 (w), 1527 (w), 1457 (m), 1378 (m), 1312 (w), 1296 (w), 1258 (w), 1226 (w), 1163 (s), 1055 (m), 1014 (w), 830 (m), 805 (w), 786 (w), 765 (w), 721 (w), 701 (w), 682 (w). Anal. Calcd for $C_{646}H_{1008}N_4O_{74}Fe_2$ (**9**-P + $10H_2O$): C, 76.62; H, 10.03; N, 0.55. Found: C, 76.48; H, 9.80; N, 0.54.

Dioxygen Reactivity Studies

Measurements were carried out in a UV–vis cell equipped with a Dewar vessel for cooling. Diiron(II) complexes were dissolved to a concentration of 0.2−0.4 mM in a drybox and loaded into the cell, which was then sealed with a septum and cooled to −29 °C in a nitromethane/dry ice bath. After the initial spectrum was recorded, O_2 gas was bubbled into the solution through a long needle for 30 s. Spectra were then recorded every 30 s for 15 min and with an increment of 20% in the cycle time thereafter. For substrate reactions, this procedure was continued for 1.5 h to achieve full conversion to the oxygenated intermediate **10**. Ar was then bubbled through the solution for 15−20 min to remove excess O_2. At this point, substrate was injected via an airtight syringe. The reaction temperature was maintained at −29 °C for 2 h, and then the solution was gradually allowed to warm up to room temperature overnight. During workup, Chelex was added to the reaction mixture, which was then stirred for two h to remove metal ions. The Chelex was filtered off and washed with a copious amount of CH_2Cl_2. The filtrates were combined, and the solvent was removed in vacuo. The products were analyzed by GC-MS with 1-bromodecane as an internal standard.

GC-MS Analyses

All gas chromatography was performed on an Agilent 6890 gas chromatograph connected to an Agilent 5973 Network mass selective detector. An HP-5ms (5%-phenyl)-methylpolysiloxane capillary column (30 m × 0.25 mm × 0.25 μm) was employed. Conditions for the 9,10-dihydroanthracene (DHA) reaction were as follows: initial temperature of 150 °C with initial time of 5 min, then the temperature was raised at 15 °C/min to 250 °C and held for a final time of 10 min. For the anthrone reaction: initial temperature = 150 °C, initial time = 5 min, ramp rate = 50 °C/min to 230 °C, final time = 10 min. Products were identified by their mass spectra and retention times compared with those of authentic samples. Quantification was made by comparison of the total ion count of the peaks interested with that of the internal standard. Calibration plots for the detector response were prepared from authentic samples of known concentration and with an internal standard.

Stopped-Flow Kinetic Studies

Kinetics experiments were carried out by using a Canterbury stopped-flow SF-40 and MG-6000 rapid diode array system (Hi-Tech Scientific) under ambient pressure. To avoid moisture and pre-oxidation, the instrument employs stainless-steel flow lines and an argon-purged anaerobic attachment. The mixing cell was maintained to ±0.1 °C. All lines of the instrument were extensively washed with dioxygen-free anhydrous solvent before experiment. Solutions of **9**-P (75.2 μM in CH_2Cl_2 before mixing) were prepared in a drybox and stored in an airtight syringe prior to loading into the stopped-flow apparatus. A saturated solution of dioxygen was prepared by bubbling the gas through CH_2Cl_2 for 20 min in a septumsealed

round-bottomed flask maintained at 20 °C, and the concentration was taken as 5.8 mM before mixing.[16] A total of 300 scans were taken within 1050 s.

Mössbauer Spectroscopy

Spectra were recorded on an MSI spectrometer (WEB Research Co.) using a ^{57}Co source in a Rh matrix. All samples were prepared with ^{57}Fe-enriched (40%) compounds. The solid sample of **9**-P was prepared by mixing ~25 mg of the compound in Apiezon N grease, coating the mixture on the lid of a nylon holder, and freezing in liquid nitrogen. The frozen toluene solution sample of **10** was prepared by the following procedure. Dioxygen was introduced into a toluene solution (400 μL) of **9**-P (~25 mg) at −29 °C. After 1.5 h, the reaction mixture was cooled in an acetone/CO_2 bath and transferred via pipet to a sample holder where the lid was permanently assembled using epoxy. The sample was then immersed in liquid nitrogen to freeze the liquid. After the measurement, the sample was warmed in the holder to room temperature for 1 h to obtain the fully oxidized product (**11**) and then frozen again for measurement. Data were collected at 4.2 K. Calibration was done with natural iron foil at room temperature for isomer shift values. The *WMOSS* plot and fit program[17] was used to fit the spectra to Gaussian lines.

Electron Paramagnetic Resonance (EPR) Spectroscopy

X-band EPR spectra were recorded on a Bruker Model 300 ESP spectrometer. The temperature was controlled with a liquid-helium EPR 900 cryostat (Oxford Instruments). Samples of **9**-P were prepared as a 1 − 1.5 mM solution in toluene or CH_2Cl_2 in the drybox. One sample was frozen to 77 K immediately when it was brought outside of the drybox. Another was cooled at −29 °C. O_2 was bubbled for 30 s through the solution, which was frozen to 77 K after 1.5 h. Spin quantification was done with copper triflate as a concentration standard. Values obtained by double integration of the signals were divided by a correcting factor that is a function of the principal *g* values.[18]

X-ray Absorption Spectroscopy (XAS)

Samples of **9**-P, **10**, and **11** were prepared as 2.56 mM solutions in toluene and kept in liquid N_2 until used. Procedures similar to those used in the Mössbauer sample preparation were adopted to generate **10** and **11**, which were then transferred to Lucite sample cells with a Kapton tape window via pipet. Samples **A**–**C** were ground with BN and pressed into a 1 mm thick Al sample holder under an inert atmosphere. The X-ray absorption spectra were recorded at the Stanford Synchrotron Radiation Laboratory (SSRL) on focused 20-pole wiggler beam line 7 −3 for **9**-P, **10**, **11**, and **C** and the 2−3 beam line for **A** and **B**, with the ring operating at 3 GeV, 50−100 mA. A Si(220) double-crystal monochromator was utilized for energy selection at the Fe K edge, detuned 50% at 8000 eV to minimize contamination of the radiation by higher harmonics on beam line 2−3. On beam line 7−3, a Rh-coated mirror upstream of the monochromator was used for harmonic rejection. The samples were maintained at 10 K during data collection by using an Oxford Instruments CF1208 continuous-flow liquid-helium cryostat. Data were measured in fluorescence mode for **9**-P, **10**, and **11** with a Canberra Ge 30-element array detector and in transmission mode for **A**-**C**, using ionization chambers filled with N_2. Internal energy calibration was performed by simultaneous measurement of the absorption of Fe foil placed between two ionization chambers located after the sample. The first inflection point of the foil was assigned to 7111.20 eV. No photoreduction effects were observed for any of the data sets. The averaged data included 33 scans for **9**-P, 21 scans for **10**, 15 scans for **11**, 11 scans for **A**, and 9 scans for **B** and **C**.

The averaged data were normalized with the program *XFIT*[19] by first subtracting a polynomial background absorbance that was fit to the preedge region and extended over the postedge with control points, followed by fitting a three-region polynomial spline of orders 2, 3, and 3 over the postedge region. The data were normalized to an edge jump of 1.0 between the background

and spline curves at 7130 eV. Theoretical extended X-ray absorption fine structure (EXAFS) signals $\chi^{(k)}$ were calculated using *FEFF* (version 7.02)[20] and fit to the data by *EXAFSPAK* (G. N. George, SSRL). The experimental energy threshold, E_0, the point at which the photoelectron wavevector $k = 0$, was chosen as 7130 eV and was varied in each fit as a common value for every component. The scale factor, S_0^2, was set to 1.0. The structural parameters that were varied during the refinements included the bond distance (R) and the bond variance (σ^2). Atom types and coordination numbers were systematically varied during the course of the analysis, but were not allowed to vary within a given fit. Data were fit over the region of $k = 2-15$ $Å^{-1}$.

The intensities and energies of the preedge features for all samples were quantified by using the fitting program *EDG_FIT* (G. N. George, SSRL) and established methodology.[21] All spectra were fit over several energy ranges (7108−7116, 7108−7117, 7108−7118, and 7108 −7119 eV), with varied backgrounds to give nine fits per sample. Each preedge feature was modeled with pseudo-Voigt line shapes of a fixed 1:1 ratio of Lorentzian to Gaussian contributions. The backgrounds were chosen to give a best fit to the preedge area while reproducing edge features. Each fit was considered successful if it simultaneously reproduced the data and the second derivative of the data over the entire energy range. The total area is the sum of the areas of all preedge features, where the area is approximated by peak height multiplied by the full width at half-maximum, scaled by 100. Error was calculated by determining the standard deviation for peak heights and half widths for each preedge feature from all successful fits.

Results and Discussion

Design, Synthesis, and Characterization of Diiron Dendrimer Complexes

The molecular design of dendritic ligands capable of assembling uniquely only two iron moieties at a central carboxylate-rich core was inspired by the family of terphenyl carboxylates.[5–7,9,10,22] The basic structure of this ligand was modified so as to incorporate convenient points for dendronization with C_{12}-terminated Fréchet-type poly(benzyl ether)dendritic wedges using a convergent approach.[23] A short synthetic route to the central core unit **4** was devised from 2,6-dibromo-3,5-dihydroxybenzoic acid as a starting material (Scheme 1).[14] Magnesium perchlorate was employed as a Lewis acid catalyst in the selective decarboxylative esterification of the benzoate functionality (**1**).[24] The phenolic moieties were then alkylated with benzyl bromide in a Williamson-type etherification facilitated by 18-crown-6 as a phase transfer catalyst. The arylation of **2** via palladium-catalyzed cross-coupling was nontrivial given the hindered nature of the reactant. After several attempts, Suzuki coupling with Pd $(PPh_3)_4$ as the catalyst demonstrated superior yields. The role of the base in this step was also noteworthy because neither Cs_2CO_3 nor K_2CO_3 gave the desired product, whereas K_3PO_4 was able to furnish **3** readily in 72% yield. The benzyl groups of **3** were removed after hydrogenolysis using Pd/C to give the central core unit poised for further dendronization.

C_{12}-terminated Fréchet-type poly(benzyl ether)dendritic wedges were chosen for the dendronization of **4** so that the fully assembled dendritic complex would be both highly globular and soluble in a range of organic solvents (Scheme 2). Our previous experience with these wedges and dendrimers thereof suggested that they would be ideal candidates for the encapsulation and protection of the diiron active site, for their performance in other catalyst constructs has been similarly successful.[15] The second-generation dendritic wedges **5** were coupled to **4** by standard methodologies,[23] giving the *tert*-butyl-protected ligands **6** in high yields. The *tert*-butyl group of **6** was then removed via thermolysis in quinoline at 220 °C to give the carboxylic acid derivative **7**. We report here diiron complexes derived from **7**.

A full comparison of compounds with both the third- and fourth-generation ligands will be made in due course.

The standard synthetic protocol for the preparation of carboxylate-rich diiron complexes involves deprotonation of carboxylic acid to ensure efficient complexation.[9] Compound **7** could not be deprotonated by NaOH at room temperature, however. A modified procedure[25] was therefore adopted, utilizing a mixed-solvent system comprising THF, water, and MeOH to make a homogeneous reaction mixture. The solution was then brought to reflux for 5 h, during which time the acid was fully deprotonated by NaOH to afford **8**. Its formation was demonstrated by loss of the C=O stretch of the free acid (1702 cm^{-1}) and the appearance of two C=O stretches arising from the carboxylate anion (1599 and 1574 cm^{-1}) in the IR spectrum. Compound **8** was then mixed with $Fe(OTf)_2 \cdot 2MeCN$ in THF for over 10 h (Scheme 3), resulting in a clear yellow solution. This behavior is the same as that observed for the simple terphenyl carboxylate $Ar^{Tol}CO_2^-$,[9] indicating the formation of the corresponding diiron complex with THF ligands. After removing the THF solvent, pentane was added and the insoluble triflate salts were filtered off. Without further purification, the filtrate was further exposed to solid 4-RPy suspended in pentanes. Unreacted 4-RPy was removed by copious pentane dissolution/filtration from the heterogeneous mixture.

The flexibility of the dendrimer unit makes it impossible to obtain crystal structures to characterize the resulting products, **9**-CN and **9**-P, but we have a sufficiently good understanding of related complexes through spectroscopic and other characterization methods that we can assign the chemical composition and probable structure with confidence. First, the elemental analyses establish the presence of one N donor and two dendrimer ligands per iron atom. Although from this information alone we cannot rule out the possibility of a mononuclear iron complex with two carboxylates and one N-donor ligand, previous work on related mononuclear Fe(II) compounds revealed that two carboxylate and two N-donor ligands are typically associated with the metal center unless the N donor is bidentate.[26] In addition, no mononuclear iron(II) complex formed when $[Fe_2(\mu\text{-}O_2CAr^{Tol})_2(O_2CAr^{Tol})_2(THF)_2]$ was allowed to react with excess 4-cyanopyridine (4-CNPy). Second, the product of the reaction of 4-CNPy with the dendrimer precursor has an optical absorbance at 463 nm (ε = 2600 $cm^{-1}\ M^{-1}$) in anhydrous CH_2Cl_2. The value is quite similar to that (λ_{max} 460 nm, ε = 2200 $cm^{-1}\ M^{-1}$) of $[Fe_2(O_2CAr^{Tol})_2(\mu\text{-}O_2CAr^{Tol})_2(4\text{-}CNPy)_2(H_2O)_2]$, a windmill-structured dinuclear species.[11,27] A more direct, third piece of evidence is provided by both X- and Q-band EPR spectra, in which a broad g = 16 signal characteristic of a coupled diiron(II) center clearly indicates the presence of a dinuclear complex (Figure S1, Supporting Information). This assignment is also consistent with the measurements described in the XAS section (vide infra). Thus, taken together, the data indicate that dinuclear windmill complexes form with the dendrimer-appended ligand. The use of water in the synthesis of **8** and the elemental analysis are consistent with the formula $[Fe_2([G\text{-}3]COO)_4(4\text{-}RPy)_2] \cdot 10H_2O$.

Dioxygen Reactivity

Reaction of a toluene solution of **9**-CN with dioxygen at −29 °C led to a slow reduction in intensity of the 475 nm absorption band with no indication of the formation of an intermediate (Figure S2, Supporting Information). The kinetics of this reaction were fit to a pseudo-first-order equation with $k_{obs} = 6.6(9) \times 10^{-4}\ s^{-1}$. The reaction of the analogous paddlewheel compound $[Fe_2(\mu\text{-}O_2CAr^{Tol})_4(4\text{-}CNPy)_2]$ with dioxygen occurs with a rate constant almost 300-fold larger at this temperature.[27] We attribute this difference to the dendrimer framework, which limits diffusion of dioxygen into the diiron core and provides an increased energy barrier for structural rearrangements that may be required for the chemistry associated with dioxygen binding.

When O_2 was bubbled into a CH_2Cl_2 solution of **9**-P at −29 °C, an optical band at 442 nm (ε = 6000 cm^{-1} M^{-1}) grew in, reaching a maximum at about 1.5 h (Figure 1a). This oxygenated intermediate, **10**, was stable as long as the temperature was maintained below −5 °C, judging by the intensity of this absorbance. The same behavior was also observed in other solvents, specifically chloroform and toluene. When Ar was used to remove excess dioxygen, the intensity of the 442 nm peak remained the same, indicating irreversible binding. Upon warming to room temperature, the absorption maximum shifted to 429 nm (ε = 5000 cm^{-1} M^{-1}), which we attribute to formation of the diiron(III) species **11**, discussed below.

Reaction of **9**-P with O_2 at 20 °C leads to the formation of **10**, which dominates the spectrum for about 100 s as indicated by its absorbance at 442 nm (Figure 1b). Compound **10** subsequently decays to **11**, overwhelming the spectral window. The intensity change at 442 nm was fit to an A → B → C process as indicated by eq 1, where $k_1' = k_1[O_2]$, since excess dioxygen ensures pseudo-first-order conditions.

$$\mathrm{Abs}_{442}(t) = [9\text{–P}]_0 \left\{ \epsilon_{11} + \left[(\epsilon_{9\text{–P}} - \epsilon_{11}) + (\epsilon_{10} - \epsilon_{11}) \frac{k_1'}{k_2 - k_1'} \right] \exp\left(-k_1' t\right) - \frac{k_1'}{k_2 - k_1'} (\epsilon_{10} - \epsilon_{11}) \exp\left(-k_2 t\right) \right\} \quad (1)$$

When $\varepsilon_{\mathbf{10}}$ and $\varepsilon_{\mathbf{9}\text{-P}}$ were fixed at 6000 and 1000 cm^{-1} M^{-1}, respectively, and the initial concentration of **9**-P was 0.0376 mM, the fit (Figure S3, Supporting Information) yielded k_1' = 0.0132(8) s^{-1}, k_2 = 0.04 (2) s^{-1}, and $\varepsilon_{\mathbf{11}}$ = 4523(5) cm^{-1} M^{-1}. The rate constants k_1' and k_2 are of the same order of magnitude, consistent with the fact that both **10** and **11** appeared within a short period of time at this temperature. This chemistry is attributed to eq 2, and the nature of **10** and **11** is further addressed below.

$$\underset{9\text{–P}}{Fe^{II}Fe^{II}} \xrightarrow[k_1]{O_2} \underset{10}{Fe^{II}Fe^{III}} - O_2 \xrightarrow{k_2} \underset{11}{Fe^{III}Fe^{III}} \quad (2)$$

Mössbauer and EPR Studies

The Mössbauer spectrum of **9**-P (Figure 2a) displays a single sharp quadrupole doublet, indicating the two iron sites to be indistinguishable. The isomer shift (δ = 1.15 mm/s) and quadrupole splitting (ΔE_Q = 2.76 mm/s) are consistent with those of high-spin diiron(II) compounds in an oxygen-rich coordination environment.[22,28]

The Mössbauer spectrum of **10** (Figure 2b) displays two quadrupole doublets, indicating two different iron sites with the isomer shift and quadrupole splitting values of δ = 1.20 mm/s, ΔE_Q = 3.10 mm/s and δ = 0.48 mm/s, and ΔE_Q = 0.71 mm/s, respectively. The fit gave a 1:1 ratio for the two sites. By comparison with the parameters reported previously, we could assign the former as a high-spin iron(II) center and the latter as a high-spin iron(III) center.[22,28] These results strongly suggest that the oxygenated intermediate **10** is a mixed-valent $Fe^{II}Fe^{III}$ species, lending further support to the assigned dinuclear structure of **9**-R. The EPR spectrum of **10** displays a weak broad absorbance at g = 2 and relatively strong signals at g = 4.24 and 4.04 (Figure S4, Supporting Information), which is typical for mononuclear Fe(III) in a rhombic environment.[29] Quantification indicated that the signals comprise less than 3.5% of total iron, the remainder being EPR-silent. This intermediate is capable of oxidizing substrates 9,10-dihydroanthracene (DHA) to anthracene and anthraquinone and also anthrone to anthraquinone, as will be discussed later. An $Fe^{II}Fe^{III}$ cation, previously generated by oxygenation of a diferrous compound, could not activate substrates because there was no oxygen-containing species bound to Fe(III).[6] We therefore believe that the $Fe^{II}Fe^{III}$ intermediate obtained here contains a reduced form of dioxygen, presumably superoxide (O_2^-), since it can perform multi-electron oxidations. In addition, the unpaired electron of a bound superoxo ion would be strongly coupled to the Fe(III) center, accounting for the absence of an EPR signal in the X-band spectrum. Intensive efforts were undertaken to detect an isotope-sensitive O–O stretching band by resonance Raman spectroscopy, but no mode could be

identified. This result may reflect either a very efficient and possibly reversible photodissociation process or the lack of an optical band involving the superoxide ion for resonance enhancement. The fact that the optical spectrum of a mixture of $Et_4N[FeCl_4]$ and 4-PPy is similar to that of **10** is consistent with the presence of an $Fe–N_{pyridine}$ bond in the latter. Recently, an oxygenated diiron(III) intermediate with no obvious optical absorbance was discovered for a transient species formed in the reaction with dioxygen of both a mutant and wild-type forms of reduced toluene/*o*-xylene monooxygenase.[30] Taken together, these results suggest that the strong absorption band observed for intermediate **10** originates from a ligand-to-metal charge transfer involving 4-PPy and Fe(III) and that no optical band derives from the superoxide ligand. Therefore, the 442 nm absorption would not provide significant enhancement to vibrations implicating the Fe–O–O fragment in a resonance Raman experiment.

When allowed to warm up, a solution of **10** decayed to the high-spin diiron(III) species **11**, for which the quadrupole splitting ΔE_Q is 0.66 mm/s and the isomer shift δ is 0.48 mm/ s. From the difference in the ΔE_Q parameters, the Fe(III) atoms in **10** and the final product must have different coordination environments.

X-ray Absorption Spectroscopy (XAS)

The Fe K-edge X-ray absorption edge shifts to higher energy from **9**-P to **10** to **11**, indicating an increase in the average iron oxidation state across the series (Figure 3). The main edge transition for **9**-P overlays well with those for the diiron(II) complexes **A** and **B** (Figure S5, Supporting Information), whereas the spectrum of **11** overlays with that for the diiron(III) complex **C** (Figure S6, Supporting Information), supporting the iron(II) and iron(III) oxidation level for **9**-P and **11**, respectively. The midway edge energy position for **10** between those for **9**-P and **11** suggests that **10** contains equal amounts of iron(II) and iron(III). A linear combination of 50% of **9**-P and 50% of **11**, however, does not reproduce the data for **10** completely (Figure S7, Supporting Information), especially in the preedge region, indicating that the iron centers in **10** are of different nature than those in the precursor and decay species.

The preedge region of the X-ray absorption spectrum is extremely sensitive to the oxidation state and geometry at an average iron site in a molecule.[21] The preedge spectrum of **9**-P consists of two peaks centered at 7111.8 and 7113.5 eV (Figure 3, inset; Table 1). This preedge energy range is characteristic of ferrous complexes, and the total preedge area of 12.3 units and the area distribution between the two peaks indicate high-spin five-coordinate iron centers in **9**-P.[21] The preedge fit for **11** reveals two peaks of comparable intensity at 7113.0 and 7114.5 eV with the total area of 7.1 units (Table 1). This energy range and area distribution are typical for high-spin ferric complexes with distorted-octahedral geometry.[21] In addition, this pattern is distinct from that observed for (μ-oxo)diiron(III) complexes,[21] and thus an oxo bridge can be ruled out for **11**. Moreover, this assignment is also consistent with the small quadrupole splitting (0.66 mm/sec) of **11** determined by Mössbauer spectroscopy; oxo bridges typically give rise to significantly larger values.[31] The preedge of **10** comprises three peaks at 7111.5, 7112.9, and 7114.3 eV, encompassing the energy regions of both iron(II) and iron(III), and thus further supporting the mixed-valent description for **10**. The relatively low total preedge intensity of 6.2 units indicates that both iron centers in **10** are in distorted-octahedral environments and contain no bridging oxo group. Finally, the highest energy peak for **10** at 7114.3 eV, which can be assigned to the iron(III) center, is shifted by 0.2 eV from the analogous peak for **11**, suggesting that the iron(III) environments are different in **10** and **11**. Hence, the Fe K preedge data indicate that both Fe(II) and Fe(III) centers in **10** are different in nature than Fe(II) in **9**-P and Fe(III) in **11**, respectively.

The Fourier transforms of the EXAFS data shown in Figure 4 illustrate major structural differences between the samples. In particular, the first-shell scattering is significantly less

intense for **9**-P than that for **10** and **11**, implying a broad distribution of the first-shell bond lengths in **9**-P. In addition, the Fourier transforms for **10** and **11** display an intense second-shell peak between 2 and 3 Å, similar to the one observed for diiron complexes and proteins with a short Fe–Fe separation[32,33] and absent in the data for the precursor **9**-P.

The EXAFS fits for **9**-P yield an average first-shell Fe–ligand distance of 2.10–2.12 Å and are significantly improved upon inclusion of a scattering component at 2.50 Å (Table 2, fits 1 and 2; Figure S8, Supporting Information). A similar component at 2.44 Å is required in the data for the dibridged $[Fe^{II}_2(\mu\text{-}O_2\text{–}CAr^{Tol})_2(O_2CAr^{Tol})_2]$ complex **A**, where it can be attributed to an average of the Fe–O and Fe–C distances of the terminal bidentate carboxylate ligand in correspondence with the crystal structure (Table S1 and Figure S9, Supporting Information). This result suggests that one terminal bidentate carboxylate per iron atom is present in **9**-P. The data for **9**-P do not accommodate a short Fe–Fe vector (fit 3), which would be representative of a tetrabridged structure similar to that of the $[Fe^{II}_2(\mu\text{-}O_2CAr^{Tol})_4]$ complex **B** with an Fe–Fe separation of 2.82 Å. Particularly, the addition of a short Fe–Fe vector in fit 3 results in a very low coordination number of 0.2 Fe and improves the fit error only marginally in comparison to that of fit 2. Since this short metal–metal distance is readily detected in the EXAFS analysis of **B** (Table S2 and Figure S10, Supporting Information), we conclude that a tetrabridged structure with a short Fe–Fe separation is incompatible with the data for **9**-P and may only be valid for 20% or less of all species in the solution. Therefore, the local structure around the iron centers of **9**-P is more similar to that of **A** than of **B**. The average Fe–ligand distances are longer for **9**-P (2.12 Å) than those for **A** (2.00 Å), reflecting steric demands imposed by the dendrimer ligands.

The first shell for the decay compound **11** can be modeled with 6 O/N ligands at 2.02 Å (Table 2, fit 6), consistent with expected bond lengths for a high-spin ferric complex. However, the shell of five Fe–C(pyridine, carboxylate) interactions at 3.00 Å has a very low Debye–Waller parameter σ^2, even when additional shells at longer distances are modeled in the fit (Table S3 and Figure S11, Supporting Information). Inclusion of an Fe–Fe vector at 3.00 ± 0.05 Å improves the σ^2 value and results in reasonable parameters for the Fe–Fe component (fit 7). This Fe–Fe distance is 0.15 Å longer than that in the tetrabridged $[Fe^{III}_2(\mu\text{-}OH)_2(\mu\text{-}O_2CAr^{Tol})_2]$ complex **C**, suggesting that the number, nature, and/or geometry of the bridging ligands are different in **11** and **C**. The Fe–Fe separation of 3.00 Å in **11** matches well the Fe–Fe distance of 2.99 Å in the oxidized form of MMOH, which features a μ-1,3 carboxylate and two hydroxo bridging ligands.[33]

The EXAFS data for the intermediate complex **10** are best modeled with 6 O/N scatterers at 2.05 Å, consistent with the intermediate valence state (Table 2, fit 4). As in the case of **11**, an Fe–Fe component at 3.05 ± 0.05 Å can be included in the second shell of the data (fit 5), improving σ^2 for the carbon shell. Although more detailed fits to the data of **10** have also been performed (Table S4 and Figure S12, Supporting Information), it is not possible to assign any of the EXAFS-derived interactions specifically to a bound superoxo ligand because of the broad range of Fe–O(carboxylate) and Fe–N(pyridine) bond lengths when Fe(II) and Fe(III) centers are simultaneously present.

Although no $Fe^{II}Fe^{III}$ superoxo intermediate has yet been detected in experimental studies of the oxygenation of nonheme diiron enzymes,[30,34] theoretical work on dioxygen activation of soluble MMOH has suggested the existence of an $Fe^{II}Fe^{III}$ superoxo species, the structure of which is portrayed in Scheme 4.[35,36] An Fe–Fe distance of 3.44 Å was computed recently by QM/MM, reduced by about 0.3 Å compared with that previously reported by a pure QM calculation.[36] Although the Fe–Fe distance from theoretical calculation for $MMOH_{red}$ agrees reasonably well with that from crystallographic studies, the value calculated for Q is significantly larger than that (2.46 Å) obtained from XAS.[36,37] It is possible to obtain shorter

values if other models are used. Therefore, intermediate **10** may bear a core structure similar to that shown in Scheme 4. We stress, however, that we do not rule out other possible binding modes for the superoxide ion. We also note the absence of an optical absorbance band at 442 nm in a published report of an η^1-superoxo iron(III) complex.[38]

Reaction of the Oxygenated Intermediate 10 with External Reagents

a. Cp^*_2Fe—Cp^*_2Fe did not react with **10** at −29 °C, judging by the failure to generate the characteristic spectrum of $Cp^*_2Fe^+$. Upon warming, however, a broad absorbance around 780 nm grew in, which is diagnostic of the decamethylferrocenium cation.[39] The relative stability of **10** toward reduction at the lower temperature may reflect the inability of Cp^*_2Fe to penetrate the dendrimer sheath at low temperatures.

b. Oxidation of 9,10-Dihydroanthracene (DHA)—DHA is a commonly used substrate for oxygenation because its weak C–H bond (BDE = 78 kcal/mol) is easy to activate.[40] After the $Fe^{II}Fe^{III}$ intermediate **10** was generated and reached its maximum concentration, Ar was bubbled through the reaction mixture for 20 min to remove unreacted O_2. DHA was then injected through an airtight syringe. The temperature was maintained at −29 °C for 2 h, and no change was observed in the UV–vis spectrum (Figure 5a). Upon warming, however, the absorption maximum began to decrease (Figure 5b), indicating reaction of the substrate with **10**. As was the case for decamethylferrocene, the diiron(II) center appears to be protected by the dendrimer shell, reacting with dioxygen only above −30 °C. The oxygenated intermediate is also very stable and does not react with substrate without warming.

After workup of the reaction mixture, the products (Scheme 5) were analyzed by GC-MS. As listed in Table 3, 13% of the substrate converts to anthracene and 25% to anthraquinone. No anthrone was detected in this experiment. Products were identified by comparing their retention times and mass spectral patterns with those of authentic standards. There were two additional small peaks in the GC trace (Figure S13, Supporting Information) that we could not identify. The mass spectrum of one showed its most intense signal at 178^+, identical to that of anthracene, and very weak signals at 194^+ and 372^+, respectively, which could arise from coupling of DHA and anthrone radicals. However, the retention time is less than that of anthrone itself. Considering the larger molecular mass expected for a coupled compound, this assignment therefore seems unlikely. The mass spectrum of another peak displayed numerous signals, and no conclusion could be drawn concerning its identity. Excluding these contributions, the mass balance was calculated to be 62%. A control experiment using the exact procedure but performed in the absence of **9**-P showed no DHA oxidation and 93% recovery of the substrate.

The generation of anthracene and anthraquinone most likely occurs via separate reaction pathways because no anthracene was oxidized to anthraquinone in a control experiment. To supply more information about the mechanism, two similar reactions were performed. In one case, Ar was not used to provide an O_2-free environment prior to substrate addition. Although the same amount of anthracene formed, production of anthraquinone was significantly decreased (Table 3). In another experiment, the reaction was brought to room temperature under Ar over a shorter period of time (15 min) after substrate addition, and yields of 11% for anthracene and 5% for anthraquinone were recorded. In an experiment where anthraquinone was used as substrate, no reaction occurred. These observations suggest that the formation of anthracene is not affected by the presence of free dioxygen or the temperature, but that the intermediate steps to form anthraquinone are greatly influenced by these factors. The decrease in oxygenated product in the presence of O_2 also suggests that radical chain chemistry, which was reported previously with a ferric bi-imidazoline complex,[41] is unlikely to be occurring here.

c. Oxidation of Anthrone Substrate—To eliminate the pathway to form anthracene, anthrone was introduced as the substrate. Similar optical changes were observed upon the introduction of dioxygen to **9-P**, generating **10**, which was stable and unreactive at low temperature for 2 h (Figure 6a). Reaction with substrate ensued when the solution was allowed to warm up (Figure 6b). Approximately 75% conversion to anthraquinone, and only this one product, was observed when Ar was used to flush free O_2 from the system prior to warm up. The higher yield strongly implies that anthrone is more reactive than DHA, perhaps because it can tautomerize to 9-hydroxyanthracene, the O–H bond in which is more readily oxidized than the C–H bond.[42] Such behavior would account for the failure to detect anthrone in the DHA reaction.

When anthrone was allowed to react with **10** in the presence of excess O_2 and with gradual warm up, however, catalytic oxidation of anthrone to anthraquinone was observed (Scheme 6), although we have no evidence that **10** is the catalyst. Table 4 lists the conditions and the product distribution for reactions occurring in CH_2Cl_2. At a higher ratio of substrate to **10**, there is significantly higher turnover. The highest turnover was obtained when the reaction was conducted at room temperature. A control experiment in the absence of **10** and in the presence of $Fe(OTf)_2{\cdot}2MeCN$ showed no conversion to product, although when 4-PPy was present there was quantitative formation of anthraquinone from anthrone. In experiments where toluene was used as the solvent, catalytic reactivity was still observed (Table 5), so it is unlikely that a solvent-derived radical is involved in the chemistry.

In order to test whether the mixed-valent intermediate **10** may promote substrate oxidation, we generated **10** with $^{18}O_2$ and conducted similar experiments. When excess isotopically labeled dioxygen was present, there was 100% incorporation of ^{18}O into the anthroquinone product. When the reaction was allowed to continue under inert gas, surprisingly, we observed ^{16}O incorporation, the source of which is unclear at this time. It is difficult to detect the product of a single turnover reaction, however, and there is usually some anthraquinone impurity in anthrone. A control experiment in which $^{18}OH_2$ was used in the preparation of **9**-P did not affect the outcome, indicating no exchange with water. Taken together, these results prevent us from assigning **10** as being responsible for the catalysis, although in a preliminary double-mixing stopped-flow experiment, where **10** was generated at 20 °C in the first chamber and mixed with anthrone after 100 s, the substrate significantly decreased the lifetime of the intermediate compared with its decay in the absence of the hydrocarbon. Further studies are planned to establish the mechanism of catalysis.

Conclusion

Dinuclear iron(II) complexes of general formula $[Fe_2([G\text{-}3]\text{-}COO)_4(4\text{-}RPy)_2]$ were successfully prepared from dendrimer-appended carboxylate ligands. The compounds were characterized by UV–vis, EPR, Mössbauer, and XAS spectroscopy in addition to elemental analysis. The oxygenation of such complexes is retarded by about 300-fold compared with that of related compounds derived from the sterically less demanding simple terphenyl carboxylate ($[G\text{-}1]COO^-$). A metastable $Fe^{II}Fe^{III}$ intermediate was detected in the reaction of $[Fe_2([G\text{-}3]\text{-}COO)_4(4\text{-}PPy)_2]$ with dioxygen. This intermediate was characterized by Mössbauer and XAS spectroscopy. Although no oxygen-sensitive band could be observed by resonance Raman spectroscopy, we formulate this intermediate as an $Fe^{II}Fe^{III}$ superoxo species because it is EPR-silent and can react with external substrates, such as DHA and anthrone, to form oxygenated products. Catalytic oxidation was discovered for anthrone reacting in the presence of the intermediate and excess O_2.

The present results provide one of few examples in non-heme diiron chemistry where external substrate oxidation can be achieved with dioxygen[43] as the terminal oxidant instead of a

peroxide.[44] In addition, the chemistry provides an $Fe^{II}Fe^{III}$ superoxo intermediate, which has been proposed in theoretical work but not yet observed for protein systems. Apparently dendritic encapsulation suppresses simple dioxygen-initiated outer-sphere one-electron oxidation to yield $Fe^{II}Fe^{III}$ mixed-valent compounds with no bound O_2 derivative, which has been reported for "smaller" diiron(II) models.[6,45] The spectroscopic characterization of this intermediate leads us to propose a bridging superoxo structure, analogous to that predicted by theory.[36] This structure differs from others by its unique μ-σ^2,σ^1 binding mode.

Supplemental Materials

Refer to Web version on PubMed Central for supplementary material.

Acknowledgment

This work was supported by grants from the National Institute of General Medical Sciences (GM32134 to S.J.L.), the National Science Foundation (DMR-0317514 to J.M.J.F.), and the Department of Energy, Office of Basic Energy Sciences through the Biomolecular Science Program at LBNL (DEAC02-05CH11231 to J.M.J.F.), and the National Institutes of Health (P41 RR001209 to K.O.H.) The Structural Molecular Biology program at SSRL is funded by the National Institutes of Health, National Center for Research Resources, Biomedical Technology Program, and the Department of Energy, Office of Biological and Environmental Research. We thank Dr. Rayane Moreira for some initial work and Dr. Shawn Burdette for initiating the collaboration between the laboratories of S.J.L. and J.M.J.F. We thank Dr. Roman Davydov and Professor Brian M. Hoffman for measuring the X- and Q-band EPR spectra of the diiron(II) compound **9**-P. This project was in part made possible by Grant Number 5 P41 RR001209 from the National Center for Research Resources (NCRR), a component of the National Institutes of Health (NIH). Its contents are solely the responsibility of the authors and do not necessarily represent the official view of NCRR or NIH.

References

1. Hecht S, Fréchet JMJ. Angew. Chem., Int. Ed 2001;40:74–91.
2. Collman JP, Fu L, Zingg A, Diederich F. Chem. Commun 1997:193–194.Jiang D-L, Aida T. Chem. Commun 1996:1523–1524.Jiang D-L, Aida T. J. Macromol. Sci. Pure Appl. Chem 1997;A34:2047–2055.Zingg A, Felber B, Gramlich V, Fu L, Collman JP, Diederich F. Helv. Chim. Acta 2002;85:333–351.
3. Bhyrappa P, Young JK, Moore JS, Suslick KS. J. Am. Chem. Soc 1996;118:5708–5711.
4. Enomoto M, Aida T. J. Am. Chem. Soc 2002;124:6099–6108. [PubMed: 12022844]
5. Lee D, Lippard SJ. J. Am. Chem. Soc 1998;120:12153–12154.
6. Lee D, Pierce B, Krebs C, Hendrich MP, Huynh BH, Lippard SJ. J. Am. Chem. Soc 2002;124:3993–4007. [PubMed: 11942838]
7. Tolman WB, Que L Jr. J. Chem. Soc., Dalton Trans 2002:653–660.
8. Lee D, Du Bois J, Petasis D, Hendrich MP, Krebs C, Huynh BH, Lippard SJ. J. Am. Chem. Soc 1999;121:9893–9894.
9. Lee D, Lippard SJ. Inorg. Chem 2002;41:2704–2719. [PubMed: 12005495]
10. Yoon S, Lippard SJ. J. Am. Chem. Soc 2004;126:2666–2667. [PubMed: 14995160]
11. Yoon S, Lippard SJ. J. Am. Chem. Soc 2005;127:8386–8397. [PubMed: 15941272]
12. Lee D, Lippard SJ. Inorg. Chem 2002;41:827–837. [PubMed: 11849083]
13. Hagen KS. Inorg. Chem 2000;39:5867–5869. [PubMed: 11151391]
14. Borchardt RT, Sinhababu AK. J. Org. Chem 1981;46:5021–5022.
15. Helms B, Liang CO, Hawker CJ, Fréchet JMJ. Macromolecules 2005;38:5411–5415.
16. Battino, R. Oxygen and Ozone. 1st ed.. Pergamon Press; Oxford and New York: p. 1981
17. Kent, TA. WMOSS, version 2.5. WEB Research Co.; Minneapolis, MN: 1998.
18. Aasa R, Vaänngård T. J. Magn. Reson 1975;19:308–315.
19. Ellis PJ, Freeman HC. J. Synchroton Radiat 1995;2:190–195.
20. Ankudinov AL, Rehr JJ. Phys. Rev. B: Condens. Matter Mater. Phys 1997;56:R1712–R1715.
21. Westre TE, Kennepohl P, DeWitt JG, Hedman B, Hodgson KO, Solomon EI. J. Am. Chem. Soc 1997;119:6297–6314.

22. Tshuva EY, Lippard SJ. Chem. Rev 2004;104:987–1011. [PubMed: 14871147]
23. Hawker CJ, Fréchet JMJ. J. Am. Chem. Soc 1990;112:7638–7647.
24. Goossen L, Döhring A. Adv. Synth. Catal 2003;345:943–947.
25. Kawa M, Fréchet JMJ. Chem. Mater 1998;10:286–296.
26. Lee D, Lippard SJ. Inorg. Chim. Acta 2002;341:1–11.Hagadorn JR, Que L Jr. Tolman WB. Inorg. Chem 2000;39:6086–6090. [PubMed: 11188526]
27. Zhao M, Song D, Lippard SJ. Inorg. Chem 2006;45:6323–6330. [PubMed: 16878942]
28. Münck, E. Physical Methods in Bioinorganic Chemistry: Spectroscopy and Magnetism. Que, L., Jr., editor. University Science Books; Sausalito, CA: 2000. p. 287-319.
29. Palmer, G. Physical Methods in Bioinorganic Chemistry: Spectroscopy and Magnetism. Que, L., Jr., editor. University Science Books; Sausalito, CA: 2000. p. 121-185.
30. Murray LJ, García-Serres R, Naik S, Huynh BH, Lippard SJ. J. Am. Chem. Soc 2006;128:7458–7459. [PubMed: 16756297]
31. Mizoguchi TJ, Davydov RM, Lippard SJ. Inorg. Chem 1999;38:4098–4103.
32. Hsu H-F, Dong Y, Shu L, Young VG Jr. Que L Jr. J. Am. Chem. Soc 1999;121:5230–5237.Hedman B, Co MS, Armstrong WH, Hodgson KO, Lippard SJ. Inorg. Chem 1986;25:3708–3711.
33. Rudd DJ, Sazinsky MH, Merkx M, Lippard SJ, Hedman B, Hodgson KO. Inorg. Chem 2004;43:4579–4589. [PubMed: 15257585]
34. Merkx M, Kopp DA, Sazinsky MH, Blazyk JL, Müller J, Lippard SJ. Angew. Chem., Int. Ed 2001;40:2782–2807.Kopp DA, Lippard SJ. Curr. Opin. Chem. Biol 2002;6:568–576. [PubMed: 12413539]Stubbe J. Curr. Opin. Chem. Biol 2003;7:183–188. [PubMed: 12714050]Moënne-Loccoz P, Baldwin J, Ley BA, Loehr TM, Bollinger JM Jr. Biochemistry 1998;37:14659–14663. [PubMed: 9778340]Riggs-Gelasco PJ, Shu L, Chen S, Burdi D, Huynh BH, Que L Jr. Stubbe J. J. Am. Chem. Soc 1998;120:849–860.Kryatov SV, Chavez FA, Reynolds AM, Rybak-Akimova EV, Que L Jr. Tolman WB. Inorg. Chem 2004;43:2141–2150. [PubMed: 15018538]
35. Gherman BF, Baik M-H, Lippard SJ, Friesner RA. J. Am. Chem. Soc 2004;126:2978–2990. [PubMed: 14995216]
36. Rinaldo D, Philipp DM, Lippard SJ, Friesner RA. J. Am. Chem. Soc 2007;129:3135–3147. [PubMed: 17326634]
37. Shu L, Nesheim JC, Kauffmann K, Münck E, Lipscomb JD, Que L Jr. Science 1997;275:515–518. [PubMed: 8999792]
38. Shan X, Que L Jr. Proc. Natl. Acad. Sci. U.S.A 2005;102:5340–5345. [PubMed: 15802473]
39. Vaucher S, Charmant JPH, Sorace L, Gatteschi D, Mann S. Polyhedron 2001;20:2467–2472.
40. Bordwell FG, Cheng J, Ji GZ, Satish AV, Zhang X. J. Am. Chem. Soc 1991;113:9790–9795.
41. Roth JP, Mayer JM. Inorg. Chem 1999;38:2760–2761. [PubMed: 11671018]
42. Roth JP, Yoder JC, Won T-J, Mayer JM. Science 2001;294:2524–2526. [PubMed: 11752572]
43. Dong Y, Ménage S, Brennan BA, Elgren TE, Jang HG, Pearce LL, Que L Jr. J. Am. Chem. Soc 1993;115:1851–1859.Carson EC, Lippard SJ. Inorg. Chem 2006;45:837–848. [PubMed: 16411722]
44. Ryu JY, Kim J, Costas M, Chen K, Nam W, Que L Jr. Chem. Commun 2002:1288–1289.Jensen MP, Lange SJ, Mehn MP, Que EL, Que L Jr. J. Am. Chem. Soc 2003;125:2113–2128. [PubMed: 12590539]Costas M, Tipton AK, Chen K, Jo D-H, Que L Jr. J. Am. Chem. Soc 2001;123:6722–6723. [PubMed: 11439071]Oldenburg PD, Shteinman AA, Que L Jr. J. Am. Chem. Soc 2005;127:15672–15673. [PubMed: 16277487]Kim J, Larka E, Wilkinson EC, Que L Jr. Angew. Chem., Int. Ed 1995;34:2048–2051.
45. Lee D, DuBois JL, Pierce B, Hedman B, Hodgson KO, Hendrich MP, Lippard SJ. Inorg. Chem 2002;41:3172–3182. [PubMed: 12054996]Hagadorn JR, Que L Jr. Tolman WB, Prisecaru I, Münck E. J. Am. Chem. Soc 1999;121:9760–9761.

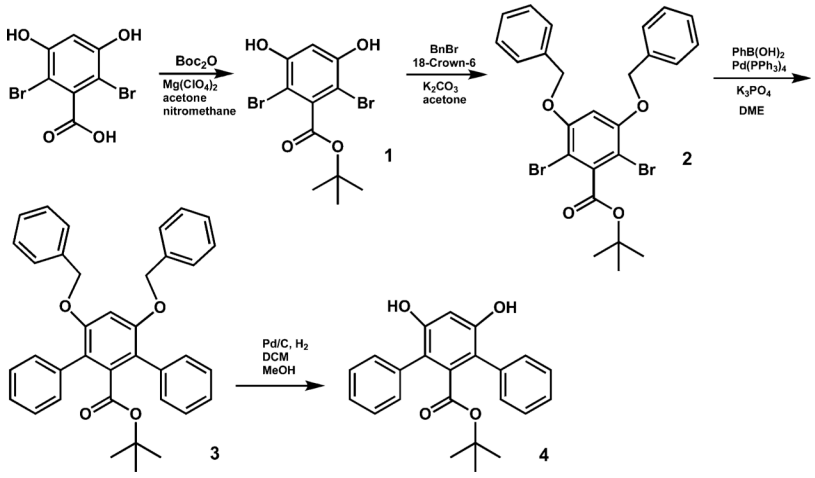

Scheme 1.
Synthetic Route to *tert*-Butyl-3,5-dihydroxy-2,6-diphenylbenzoate, **4**

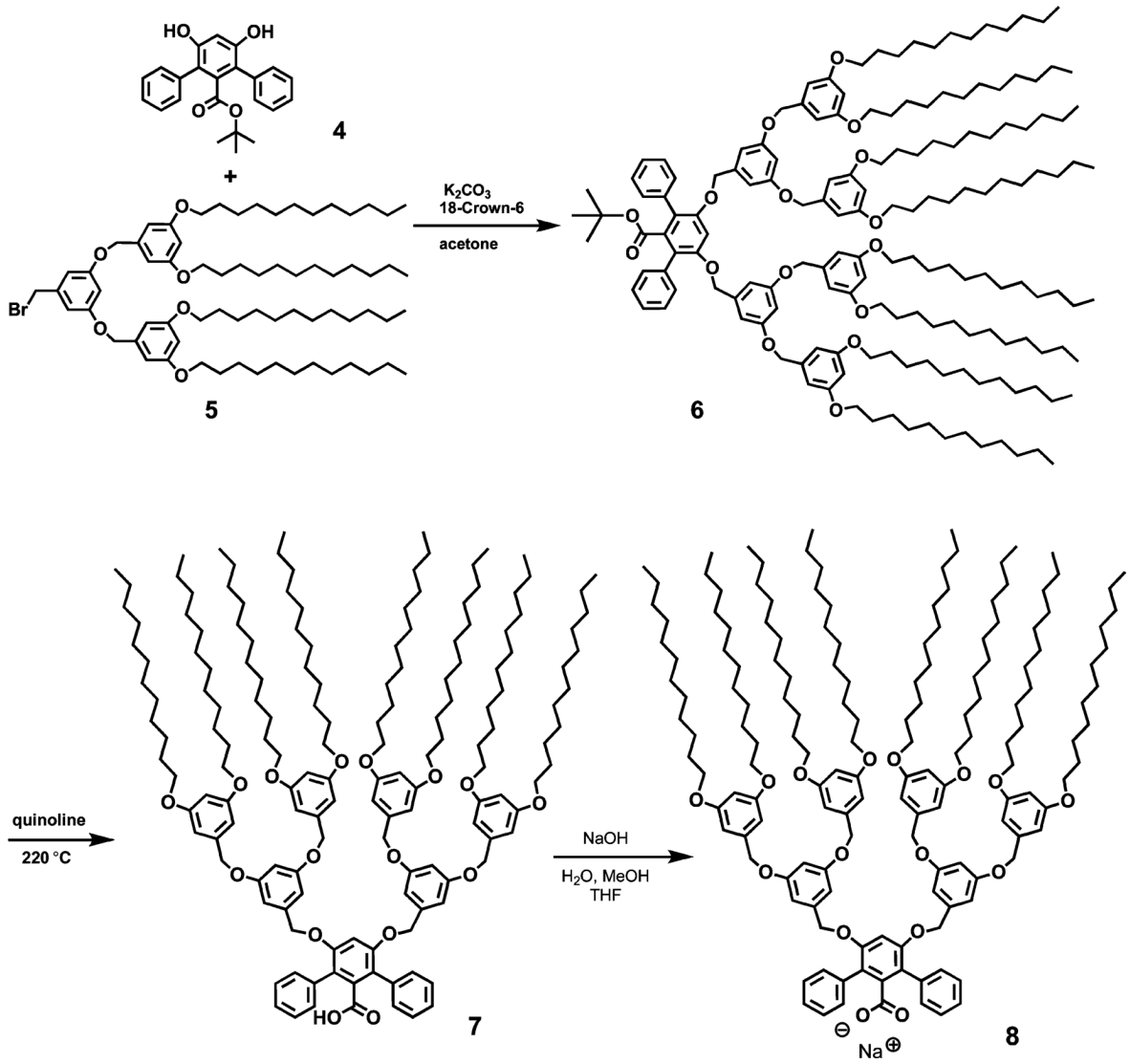

Scheme 2.
Synthesis of the Third-Generation Dendrimer-Appended Carboxylate Ligand

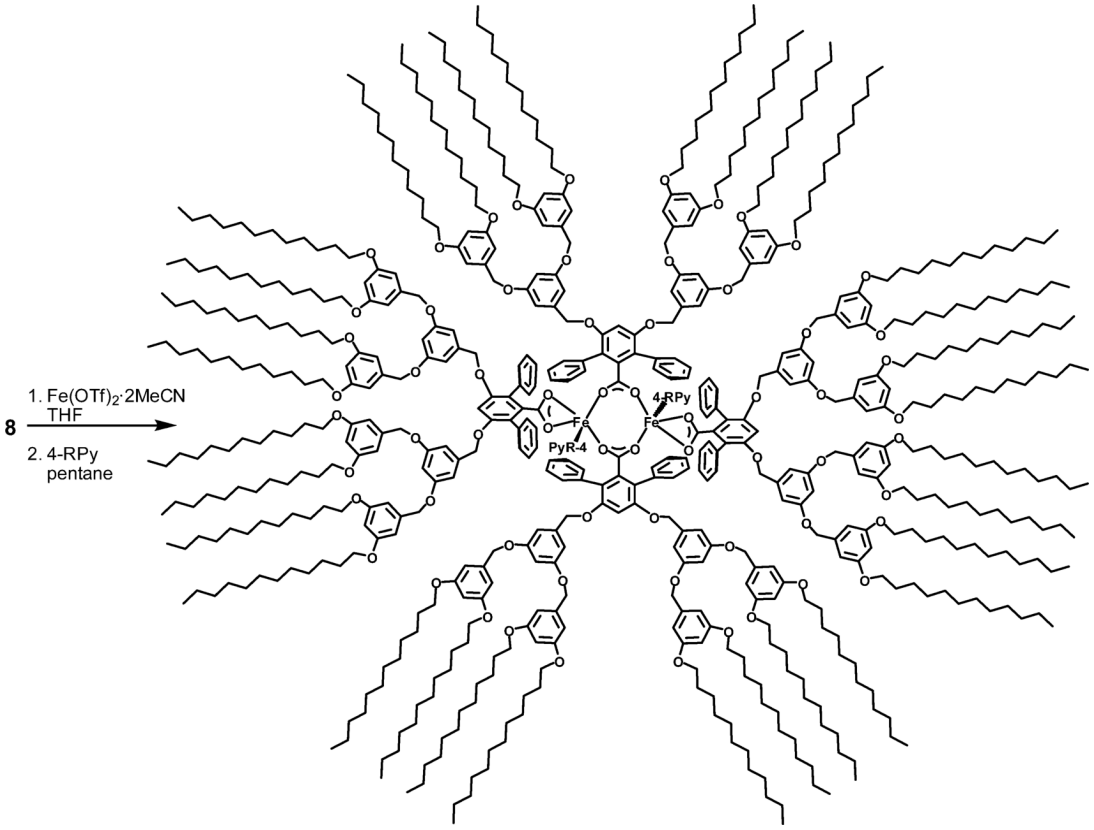

Scheme 3.
Synthesis of Dendrimer-Appended Diiron(II) Complexes **9**-R

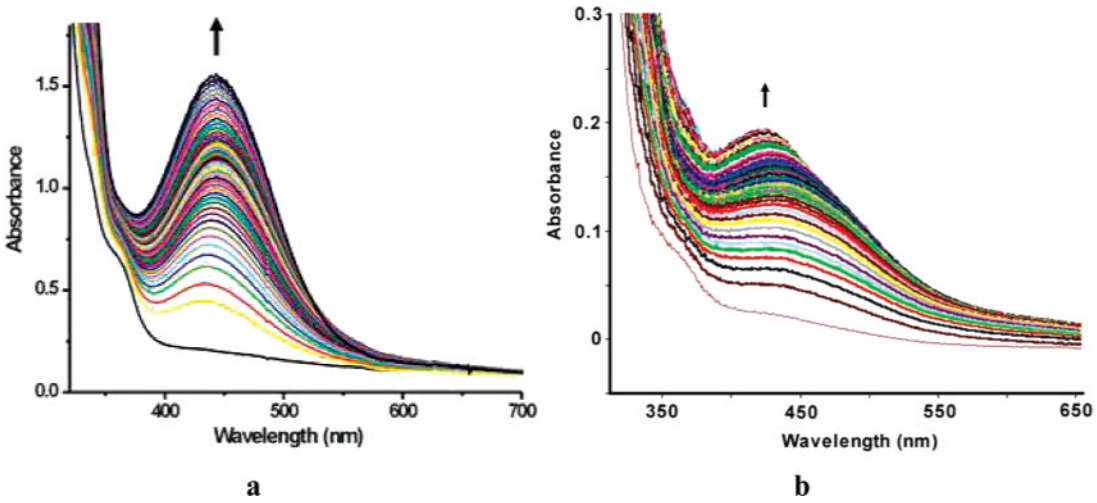

Figure 1.

Optical changes observed when **9**-P reacts with O_2 in CH_2Cl_2. (a) At −29 °C (0.252 mM). Spectra were recorded every 30 s up to 15 min and with an increment of 20% in the sampling thereafter. (b) At 20 °C (0.0376 mM). A total of 300 scans were taken in 1050 s.

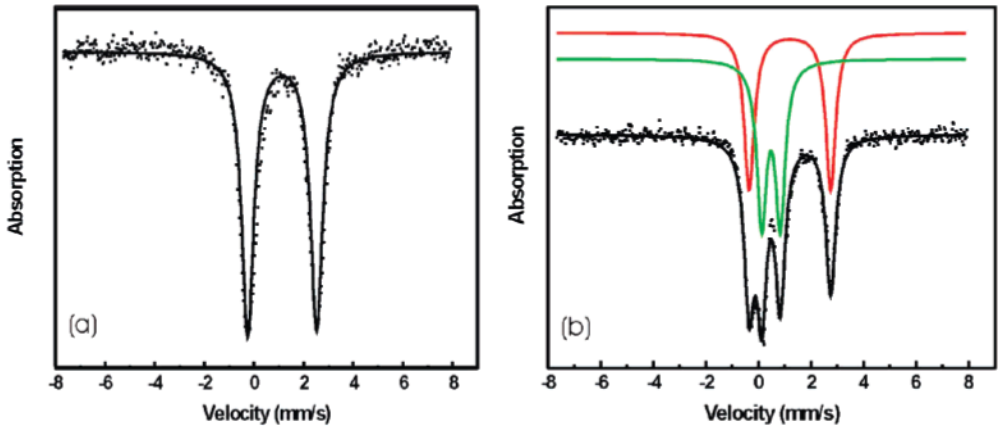

Figure 2.
Mössbauer spectra of (a) **9**-P and (b) oxygenated intermediate **10**. The experimental data are displayed as dots, and the fits are displayed as solid lines.

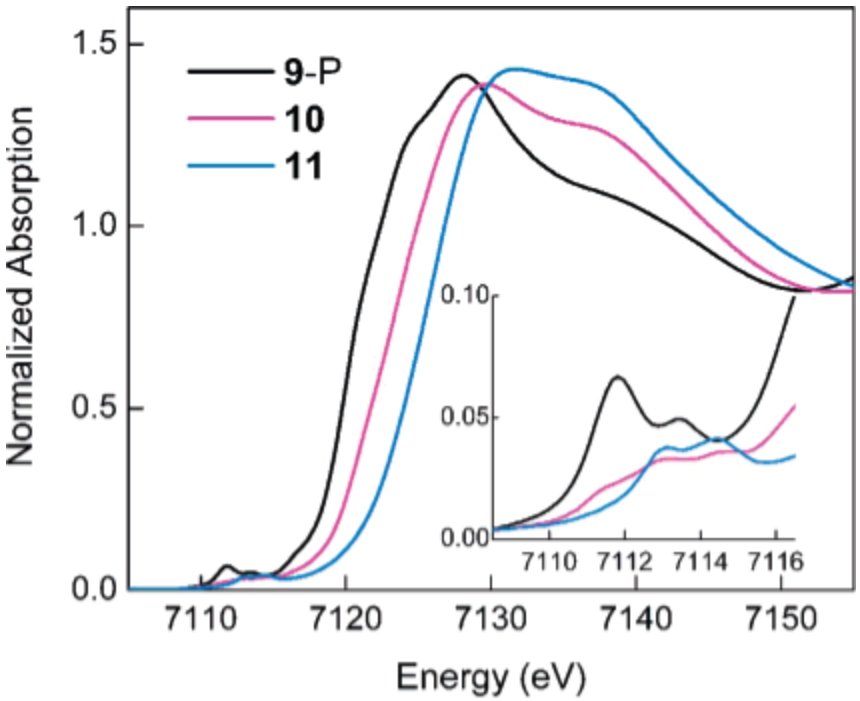

Figure 3.
Fe K-edge spectra for **9**-P, **10**, and **11**. The inset shows the magnified preedge region.

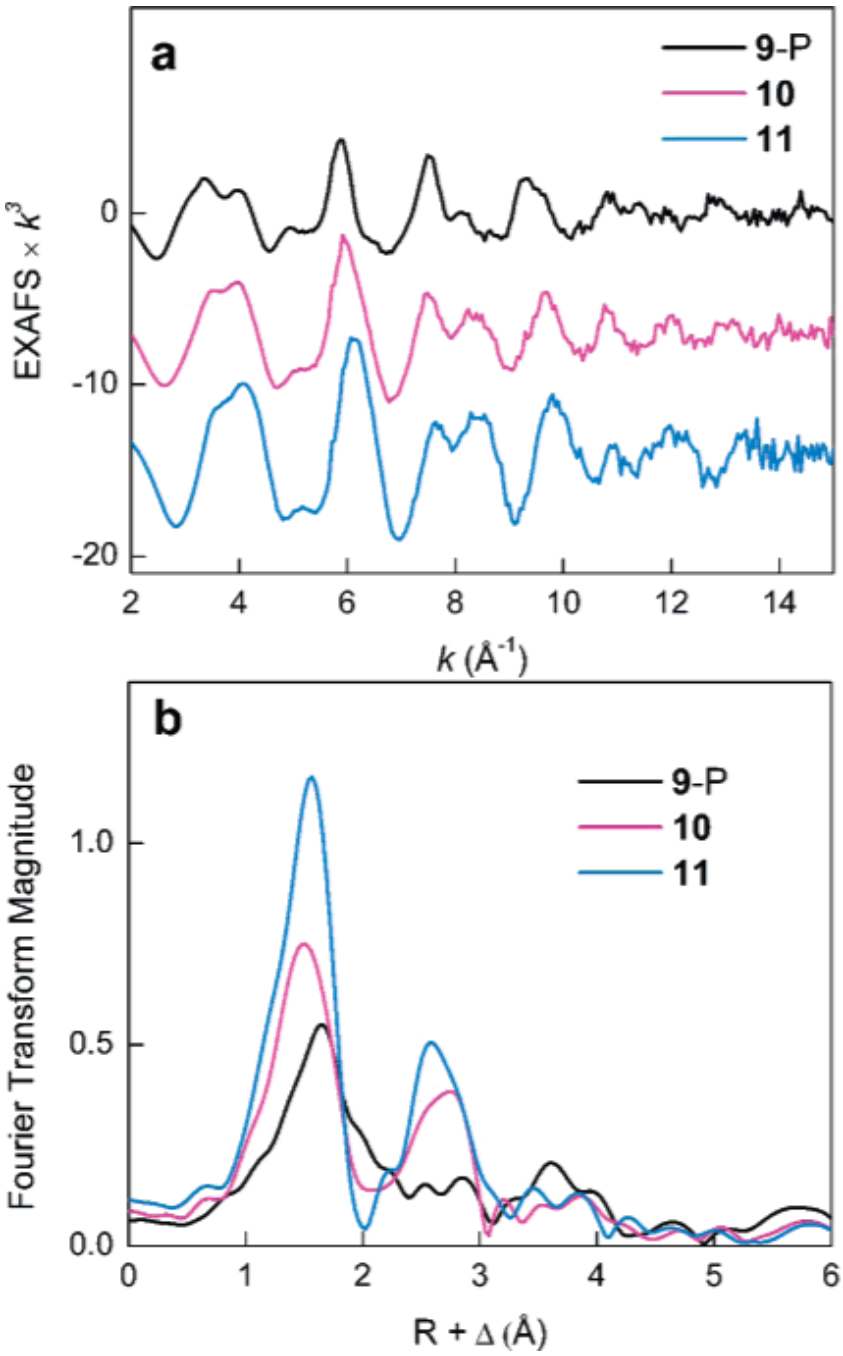

Figure 4.
(a) Fe K-edge EXAFS data for **9**-P, **10**, and **11**. (b) Fourier transforms of the EXAFS data.

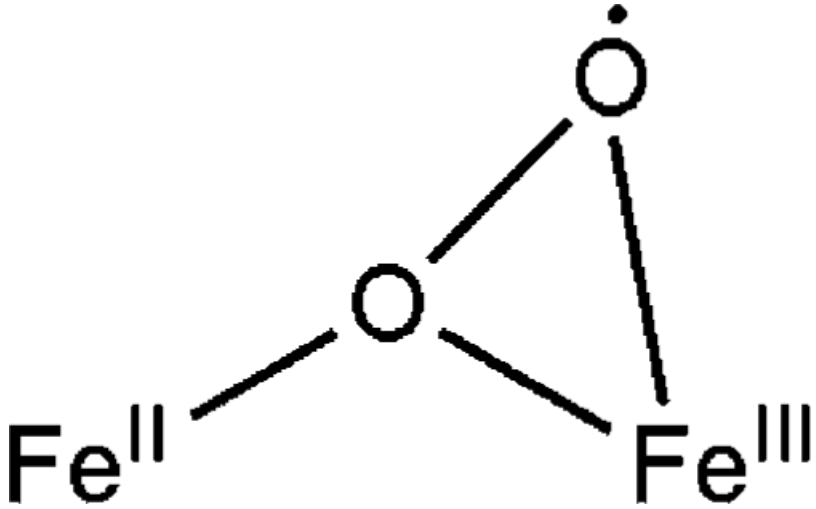

Scheme 4.
Possible Structure of the $Fe^{II}Fe^{III}$ Superoxo Intermediate **10**

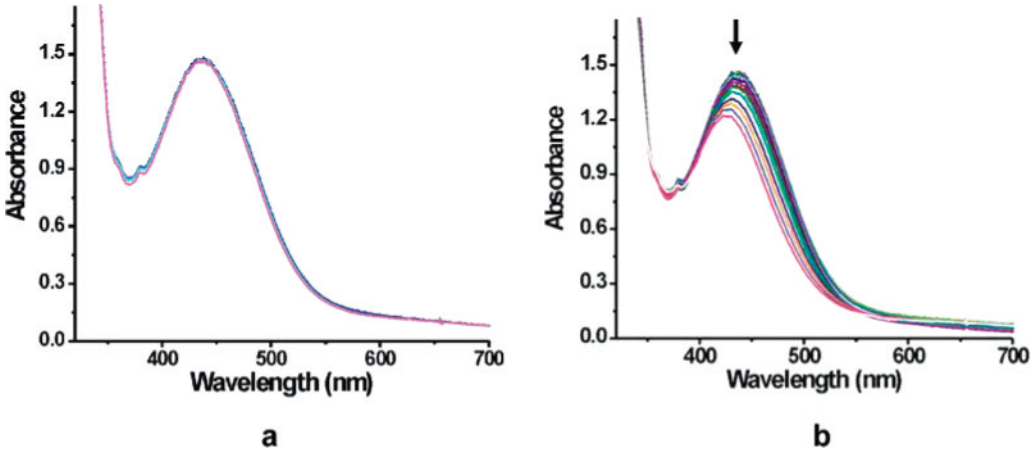

Figure 5.
Optical changes observed when **10** reacted with DHA (a) at −29 °C for two h and (b) upon warming to room temperature.

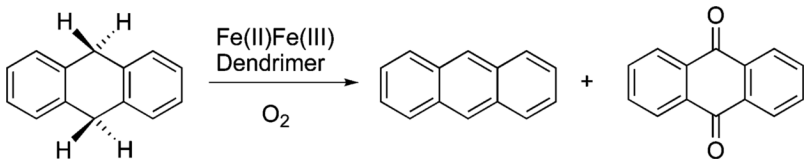

Scheme 5.
Oxidation of DHA in the Presence of $Fe^{II}Fe^{III}$ Species **10** and O_2

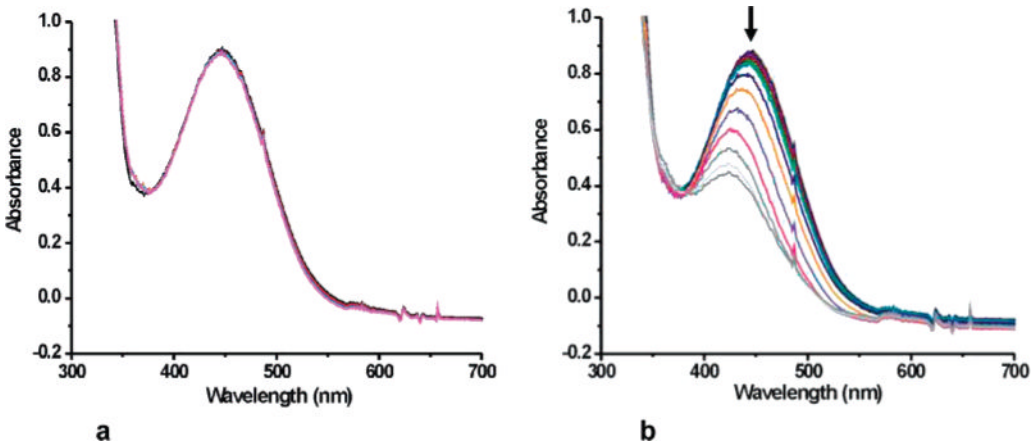

Figure 6.
Optical changes observed when **10** reacted with anthrone (a) at −29 °C for 2 h and (b) upon warming to room temperature.

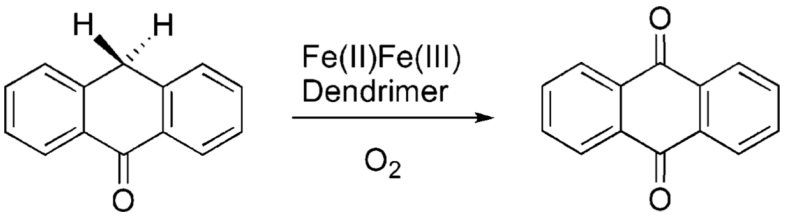

Scheme 6.
Catalytic Oxidation of Anthrone to Anthraquinone in the Presence of **10** and O_2

Table 1

XAS Preedge Fit Results for 9-P, 10, and 11

sample	preedge peak energy	preedge peak intensity[a]	total preedge peak intensity[a]
9-P	7111.8 (0.01)	9.0 (0.1)	12.3 (0.2)
	7113.5 (0.01)	3.3 (0.2)	
10	7111.5 (0.01)	1.8 (0.1)	6.2 (0.1)
	7112.9 (0.01)	2.7 (0.1)	
	7114.3 (0.01)	1.7 (0.1)	
11	7113.0 (0.03)	4.1 (0.1)	7.1 (0.5)
	7114.5 (0.01)	3.1 (0.6)	

[a]Values reported for the preedge intensity are multiplied by 100 for convenience.

Table 2

EXAFS Curve-Fitting Results for **9**-P, **10**, and **11**[a]

sample	fit no.		R (Å)	$\sigma^2 \times 10^6$ (Å^2)	ΔE_0 (eV)	F[b]
9-P	1	5 O/N[c]	2.10	1200	−6.2	0.497
		4 C	3.06	660		
	2	4 O/N	2.12	900	−3.9	0.400
		2 C/O	2.50	830		
		4 C	3.07	600		
	3	4 O/N	2.12	900	−3.8	0.393
		2 C/O	2.49	860		
		0.2 Fe	2.92	650		
		4 C	3.09	510		
10	4	6 O/N	2.05	1300	0.7	0.331
		5 C	3.04	340		
	5	6 O/N	2.05	1280	0.1	0.280
		1 Fe[d]	3.03	400		
		5 C[d]	3.00	1520		
11	6	6 O/N	2.02	840	0.7	0.298
		5 C	3.00	270		
	7	6 O/N	2.02	820	0.0	0.241
		1 Fe[d]	3.00	400		
		5 C[d]	2.94	1160		

[a] Errors are estimated to be 25% for coordination numbers and 0.01 − 0.03 Å for distances.

[b] Error (F) is defined as $F = [\Sigma k^6(\chi_{exptl} - \chi_{calcd})^2]/\Sigma k^6|\chi_{exptl}|^2]$.

[c] Scatterers differing by $Z = \pm 1$ are not distinguishable by EXAFS. The first element in a pair indicates the type of atom used to model the backscattered wave in the theoretical fit.

[d] Due to a high degree of correlation, the errors for the Fe—Fe and Fe—C distances at ~3.0 Å are estimated to be around 0.05 Å.

Table 3

Product Distribution in the Reaction of DHA with **10**, Which Was Generated at −29 °C, Followed by Substrate Addition at The Same Temperature

reaction conditions	anthracene (%)	anthraquinone (%)[a]
Ar, warm up from −29 °C to RT over 12 h	13	25
O_2, warm up from −29 °C to RT over 12 h	13	9
Ar, warm up from −29 °C to RT over 15 min	11	5

[a] Product yield was calculated based on **10**.

Table 4

Product Distribution When Anthrone Was Allowed to Reacted with **10** in CH_2Cl_2. The Yields Were Calculated Based on Substrate

substrate/10	anthraquinone (%)	turnover
11:1	53	5.6
18:1	53	9.5
129:1	11	14
103:1 (RT)	43	44

Table 5

Product Distribution When Anthrone Was Allowed to React with **10** in Toluene. The Yields Were Calculated Based on Substrate

reaction condition	substrate/10	anthraquinone (%)	turnover
−29 °C, slowly warm	10.5:1	30	3.2
RT	103:1	24	25
71 °C	124:1	13	16